RETRIEVAL OF PRECIPITATION PROFILES FROM MULTIRESOLUTION, MULTIFREQUENCY, ACTIVE AND PASSIVE MICROWAVE OBSERVATIONS

Mircea Grecu

Goddard Earth Sciences and Technology Center, University of Maryland Baltimore County
Baltimore, MD

Emmanouil N. Anagnostou

Department of Civil and Environmental Engineering,
University of Connecticut
Storrs, Connecticut

William S. Olson

Joint Center for Earth Systems Technology, University of Maryland, Baltimore County and
NASA Goddard Space Flight Center
Greenbelt, Maryland

Submitted to *Journal of Applied Meteorology*
August 2002

Corresponding Author:

Dr. Mircea Grecu
GEST/ UMBC
NASA Goddard Space Flight Center
Code 912.0
Greenbelt, MD 20770
Email: grecu@agnes.gsfc.nasa.gov
Tel: (301) 614-6322

Abstract

In this study, a technique for estimating vertical profiles of precipitation from multifrequency, multiresolution active and passive microwave observations is investigated using both simulated and airborne data. The technique is applicable to the Tropical Rainfall Measuring Mission (TRMM) satellite multi-frequency active and passive observations. These observations are characterized by various spatial and sampling resolutions. This makes the retrieval problem mathematically more difficult and ill-determined because the quality of information decreases with decreasing resolution.

A model that, given reflectivity profiles and a small set of parameters (including the cloud water content, the intercept drop size distribution, and a variable describing the frozen hydrometeor properties), simulates high-resolution brightness temperatures is used. The high-resolution simulated brightness temperatures are convolved at the real sensor resolution. An optimal estimation procedure is used to minimize the differences between simulated and observed brightness temperatures. The retrieval technique is investigated using cloud model synthetic and airborne data from the Fourth Convection And Moisture Experiment. Simulated high-resolution brightness temperatures and reflectivities and airborne observations are convolved at the resolution of the TRMM instruments and retrievals are performed and analyzed relative to the reference data used in observations' synthesis. An illustration of the possible use of the technique in satellite rainfall estimation is presented through an application to TRMM data.

The study suggests improvements in combined active and passive retrievals even when the instruments' resolutions are significantly different. Future work needs to better quantify the retrievals' performance, especially in connection with satellite applications, and the uncertainty of the models used in retrieval.

1. Introduction

Past studies demonstrated various ways in which passive microwave information can contribute to the improvement of airborne and satellite-borne radar precipitation estimates. A straightforward option to include radiometer information in algorithms for precipitation estimation from space-borne and airborne radar observations, such as those provided by the Tropical Rainfall Measuring Mission (TRMM) precipitation radar (PR), is the estimation of the Path Integrated Attenuation (PIA) at the radar's frequency from radiometer observations. Because the PIA affects the radar precipitation estimates in a twofold way, through the reflectivity profile corrected for attenuation but also through the reflectivity-precipitation relationships that are updated as a function of PIA, the accuracy of the PIA estimation considerably affects the precipitation estimation. Estimates of PIA based exclusively on the reflectivity profiles are quite uncertain due to variations in the drop size distributions (DSD) and independent considerations need to be taken into account to reduce the PIA uncertainty to acceptable levels. Meneghini et al. (2000) used a Surface Reference Technique (SRT) to estimate the PIA, while Smith et al. (1997) inspired by the work of Weinman et al. (1990) derived formulations to estimate the PIA from 10 GHz radiometer observations. The benefit of using radiometer based estimates of PIA in radar profiling algorithms has not been fully investigated, but at least theoretically the radar-radiometer estimates may lead to better results than the SRT estimates alone. Another way of including passive observations in radar rain profiling algorithms is by iteratively modifying the radar retrievals as a function of a small number of parameters (able to provide a large number of possible solutions given a profile of attenuated reflectivity) until the differences between calculated and observed brightness temperatures reach a certain minimum. This kind of approach was explored by Grecu and Anagnostou (2002). Similar, but not fully equivalent, approaches were investigated by Schols and Weinman (1994), Olson et al. (1997), Meneghini et al. (1997), and Marzano et al. (1999).

One common characteristic of most combined approaches is that they were investigated using airborne data, assuming similar resolutions and coincidence for all observations. Other approaches such as the combined TRMM algorithm (Haddad et al. 1997) account for the differences in sensors' resolutions but have not been fully characterized with respect to radar-only retrievals. In particular, the combined TRMM algorithm uses a priori brightness temperature-attenuation relationships independent of the vertical variability of the actual profiles being retrieved (Haddad et al. 1997) and, consequently, might not completely benefit from the information provided by passive observations. This justifies the investigation of a more general retrieval technique from passive and active observations at the TRMM sensors' resolutions.

The purpose of this paper is to provide such an investigation. The study is based on both cloud model simulated and airborne data. That is, cloud model produced databases are used to generate observations similar to satellite observations, in particular TRMM's, and a combined technique, which is an extension of that formulated by Grecu and Anagnostou (2002), is used to retrieve precipitation profiles from active and passive observations. The combined technique is based on radar and radiometer simulation models and uses an optimal estimation formulation to minimize the differences between observations and simulations of brightness temperatures. A more detailed description is given in the next section. The retrievals are compared to the actual profiles used in the observation synthesis, and the retrieval performance is assessed based on these comparisons. Similarly, airborne data from the Fourth Convection and Moisture Experiment (CAMEX-4) are used to generate TRMM-like observations. The combined technique is applied to these observations and indirect criteria, such as the agreement between simulated and observed brightness temperatures at the initial airborne instruments' resolutions, and the agreement between retrieved and SRT PIAs, are used to analyze the technique's performance. The potential use of the technique is illustrated using an application to actual

TRMM observations. This application is meant to give some sense of the technique's utility in satellite applications, but significant additional work needs to be done before some definite conclusions may be drawn.

The paper is organized as follows. The next section describes the mathematical formulation of the combined technique. Section 3 contains results from a simulation experiment, i.e. the application of the technique to synthetic observations generated using cloud model data and the analysis of the retrievals. In Section 4, the technique is applied to airborne data originating from CAMEX-4. The application to TRMM data is presented in section 5, and conclusions and recommendations for future work are provided in Section 6.

2. Formulation of the combined retrieval technique

The retrieval technique is an extension of the one formulated by Grecu and Anagnostou (2002). The basic radar and radiometer modeling components are essentially the same, the major difference being an adaptation of these basic components to be consistent with the characteristics of TRMM's sensors. In the earlier work, each precipitation profile could be retrieved independently of other precipitation profiles. In the current formulation, given the overlapping of passive sensor footprints, a simultaneous retrieval of a large number of profiles (encompassing large areas of precipitation) must be considered. This will become more evident in subsequent paragraphs.

As remarked by Grecu and Anagnostou (2002), although the most rigorous formulation requires the quantification and inclusion of all radar observational and modeling uncertainties, a simplified formulation is preferable because it makes the solution computationally more tractable. Consequently, we consider for each precipitation profile a small set of parameters that influence the radar retrieved profiles or the brightness temperature simulations. This set includes the intercept of the

DSD, N_0^*, a variable describing the cloud water content, x_c, and the ratio of snow to graupel content above the melting layer, x_s. There are obviously other variables that influence the radar retrievals and the radiative transfer calculations, but their effect is somewhat smaller. Consequently, to make the problem better posed (with a more specific solution) we choose not to include the less significant variables in the formulation.

The drop sizes are assumed to follow a normalized gamma distribution (Testud et al. 2000). This kind of formulation is flexible and allows a simple parameterization of variability in relationships between various precipitation-related variables. The cloud water content variable, x_c, is a proportionality parameter that multiplied by a mean cloud profile provides the vertical distribution of cloud water content. The ratio of snow to graupel content, denoted x_s, is introduced to account for the impact of frozen hydrometeor density on the scattering properties.

Given these variables, i.e. $\mathbf{X}_R = \{N_O^*, x_c, x_s\}$, and the reflectivity profiles, we simulate brightness temperatures at the radar resolution. Then, we convolve the brightness temperatures at the resolution of the TRMM sensors, and based on the differences between simulations and observations, we update the values of $\mathbf{X_R}$. The radar retrieval algorithm and the radiative transfer model are fully described in Grecu and Anagnostou (2002). A bayesian formulation, similar to that in Grecu and Anagnostou (2002) but extended to account for the space-borne sensor resolution may be derived in terms of a functional that provides an optimal estimation through its minimization:

$$
\begin{aligned}
F = \frac{1}{2}\left(\mathbf{T_B^M} - \int_E \mathbf{G}(A)\mathbf{T}_{B\,A}(A, \tilde{\mathbf{X}}_Q, \tilde{\mathbf{X}}_R)dA \right)^T \mathbf{W}_T^{-1} \left(\mathbf{T_B^M} - \int_E \mathbf{G}(A)\mathbf{T}_{B,A}(A, \tilde{\mathbf{X}}_Q, \tilde{\mathbf{X}}_R)dA \right) \\
+ \frac{1}{2}\left(\mathbf{M}_{XR} - \tilde{\mathbf{X}}_R\right)^T \mathbf{W}_{XR}^{-1}\left(\mathbf{M}_{XR} - \tilde{\mathbf{X}}_R\right) + \\
+ \frac{1}{2}(\mathbf{PIA}_S - \mathbf{PIA}(\tilde{\mathbf{X}}_Q, \tilde{\mathbf{X}}_R))^T \mathbf{W}_{PIA}^{-1}(\mathbf{PIA}_S - \mathbf{PIA}(\tilde{\mathbf{X}}_Q, \tilde{\mathbf{X}}_R))
\end{aligned}
\tag{1}
$$

In Eq. (1), $\mathbf{T}_B^M$ is a two dimensional array of co-located brightness temperatures, E is the region viewed by the instruments, **G** is the antenna gain function, $\mathbf{T}_{B,A}$ is an array of brightness temperatures calculated from radar retrievals, $\tilde{\mathbf{X}}_Q$ is an array of radar retrieved hydrometeor contents, $\tilde{\mathbf{X}}_R$ is an array of $\mathbf{X_R}$ vectors and $\mathbf{M_{XR}}$ is an a priori estimate of $\tilde{\mathbf{X}}_R$. The variable A under the integral is a dummy variable indicating an elemental area in the sampling area E. For example, in the TRMM retrieval problem, dA is the PR's footprint. In the third term of F, **PIA** is the model predicted array of PIA, $\mathbf{PIA_s}$ is a surface return based estimate of PIA, while all variables denoted **W** are covariance matrices indicating the confidence in observations and simulation models. Details regarding the methodology of specifying the covariance matrices and the a priori estimates are given in the next section.

To determine the set of radar profiles and associated brightness temperatures considered in (1) in a given meteorological context, two simple rules derived from an optimality principle are used. These rules are: 1) any two precipitation profiles located in a common passive observation footprint must be simultaneously retrieved and 2) any two overlapping passive observations must be considered together in (1) if there is precipitation in the overlapping region. If the simultaneous application of these two rules leads to a formulation involving too large a number of variables to allow a solution using the current computational resources, the functional F is separated in two or more sub-functionals and retrievals are performed for each of them. For example, in TRMM applications we do not perform retrievals involving more than 500 PR consecutive scans, i.e. 49x500 pixels, but reduce the problem to sub-problems that satisfy this size requirement.

It may be noted that the functional F in (1) depends only on $\tilde{\mathbf{X}}_R$ because $\tilde{\mathbf{X}}_Q$, i.e. the radar-retrieved hydrometeor contents, can be determined uniquely as a function of reflectivity profiles and

$\tilde{\mathbf{X}}_R$. The large-scale optimization problem associated with the minimization of functional F is addressed using a gradient-based procedure. The minimization procedure and means of efficiently evaluating the functional gradient are described in Grecu and Anagnostou (2002). In the next section, we investigate the combined retrieval technique through a simulation-based experiment.

3. Simulation results

In this section, we synthesize TRMM-like observations using cloud-resolving-model (CRM) simulated data. Retrievals are performed from the synthetic observations and the CRM data are used as a reference to assess the retrievals' performance. The cloud data for the simulation experiment is derived from a simulation of Hurricane Bonnie (August, 1998), performed using the Penn State/NCAR mesoscale model MM5. MM5 employs bulk parameterizations, which constitutes a limitation in exploring the impact of DSDs' variability on retrievals, but nevertheless is one of the best options, given that explicit microphysics schemes are extremely intensive from the computational point of view.

The brightness temperature simulations are performed using a modified Eddington model (Bauer et al. 1998). That is, the slant-profiles of hydrometeors corresponding to the instrument pointing vectors are sampled from the CRM 3-D grid, and the Eddington approximation is applied. Everything else regarding the radiative transfer calculations is the same as in Grecu and Anagnostou (2002). The brightness temperature calculations are done at the CRM's resolution (2 km). The DSD intercept, N_0^*, is generated at random but assuming the horizontal correlation and typical values determined by Testud et al. (2000). The high-resolution brightness temperatures are convolved at TRMM sensors' resolutions using Gaussian functions consistent with the sensors' characteristics as specified in Kummerow et al. (1997). The sampling resolution of TRMM Microwave Imager (TMI) is

also considered in the observation synthesis. The pseudo TMI observations are generated on a grid of approximately 15 km in the along track direction and 9 km (4.5 km for the 85GHz observations) in the across track direction. The precipitation radar (PR) observations are generated consistently with TRMM PR sampling resolution (approximately on a 4.5 km x 4.5 km grid).

The covariance matrices and the a priori estimates, $\mathbf{W}$ and $\mathbf{M_{XR}}$ in Eq. (1), are set through a methodology similar to that of Grecu and Anagnostou (2002). $\mathbf{W_{XR}}$ and $\mathbf{M_{XR}}$ are evaluated directly from the cloud model simulated data, assuming that the best a priori estimate of $\mathbf{X_R}$ is its mean over all values produced by the cloud model simulations. Variable x_c is determined as the first component in an empirical orthogonal function (EOF) decomposition. In other words, the cloud water content profile is represented as a linear combination of orthogonal vertical profiles that are the eigenvectors of the covariance matrix determined by all cloud water content profiles in the cloud database. The advantage of such a representation resides in the fact that the first few eigenvalues and their associated coefficients explain most of the profiles' vertical variability (in other words a more economical representation of cloud water profiles is achieved). Variable x_s is simply taken as the vertical mean ratio of snow to graupel content $\mathbf{W_{PIA}}$ is set to 4.0 dB^2 as suggested by the findings of Meneghini et al. (2000). Matrix $\mathbf{W_T}$ is probably subject to the largest uncertainties of all covariance matrices. This is because, in spite of numerous studies carried out to quantify the uncertainties associated with radiative transfer calculations in precipitating clouds, there are still issues that need to be further addressed. These include the modeling of the bright band (Olson et al., 2001), the quantification of the three-dimensional effects on the polarized transfer of radiation (Roberti and Kummerow 1999), parameterization of the effect of precipitation small-scale variability on calculated brightness temperatures (Harris and Foufoula-Georgiou, 2000) etc. Unfortunately, from the point of view of quantifying the uncertainties in radiative transfer calculations in precipitating clouds, the existing

studies are still preliminary. We therefore consider in this experiment only the uncertainties introduced in radiative transfer calculations by various parameterizations used to make the problem better defined and computationally less intensive. No potentially systematic errors caused by the bright band model (from Grecu and Anagnostou 2002), three-dimensional effects other than those mitigated by the slant-model, raindrop oblateness, small-scale variability, etc. are considered. Other errors, resulting from the simplified representation of the vertical variation of cloud water content and ratio of snow to graupel by just two variables, x_c and x_s, are investigated and included in $\mathbf{W_T}$. Additional uncorrelated, random errors with 0 mean and 1 K standard deviation (Marzano et al. 1999), accounting for observational uncertainty, are considered in $\mathbf{W_T}$.

The following scenario is considered in the synthetic retrieval experiment. The radar and radiometer observations are synthesized as described above. PIA estimates, as provided by a surface reference technique are generated with the addition of errors to the actual PIA's determined in the radar observations' synthesis. The errors are assumed to be spatially correlated with a decorrelation distance, i.e. the distance beyond which the correlation drops below 0.5, of 30 km. Other decorrelation distances are investigated as well and the results will be mentioned in subsequent paragraphs. The errors in surface-return estimates of PIA are likely to be correlated. This is because the surface reflectivities are correlated and a factor that causes an error (like the variation of surface wind speed, for example) in the estimation of the rain-free surface return at a certain location and further translates to an error in the PIA estimate is likely to manifest itself at adjacent locations as well. The mean PIA error is 0dB and its standard deviation is 2 dB. Only polarization corrected brightness temperatures (PCTs, defined as $1.818T_V$-$0.818T_H$, where T_V and T_H are the vertically and horizontally polarized brightness temperatures) are considered in the retrieval. The 21.3 GHz channel constitutes an exception, because only the vertically polarized brightness temperature is sensed at that frequency, and

consequently PCT may not be derived. The reason for considering PCT's is that they are somewhat less sensitive to uncertainties in surface emissivities than vertically and horizontally polarized brightness temperatures. The fact that the number of radiometer observations is reduced about two times when considering PCT's does not constitute a significant deterioration of the initial information quality, because the horizontally and vertically polarized brightness temperature are strongly correlated and the polarization signature, i.e. the difference between the two polarization temperatures, may not be correctly reproduced by an Eddington model (Roberti and Kummerow, 1999). Random errors, with 0 mean and 2 K standard deviation were added to the synthetic brightness temperature observations to account for random errors in the radiative transfer calculations.

The retrieval performance, in terms of error histograms for various retrieved variables are given in Fig. 1. Two sets of curves are presented in this figure. One corresponds to radar-only retrievals (symbolized with dashed lines), while the other corresponds to combined retrievals. It is apparent in Fig. 1 that the errors associated with the combined retrievals are smaller than those produced by radar-only retrievals. The histogram of PIA errors for radar-only retrievals is bimodal, because for low PIA values the analytical estimate from the reflectivity profile is weighed more than the SRT estimate. This procedure is similar to that employed by the actual TRMM PR algorithm (see Iguchi et al. 2000). For large PIA values, the analytical estimate weighs little and the solution substantially depends on the surface return technique. The PIA error is smaller for combined retrievals than for radar-only retrievals, i.e. the number of retrievals with absolute errors less than 0.5 dB increases, while the number of retrievals with errors larger than 0.5 dB decreases. It is also apparent from Fig. 1 that the improvement in PIA estimation translates to improvements in N_0^* and surface rain estimation. (Parameter dN is defined here as the ratio of retrieved N_0^* to actual N_0^*.) In addition to improvements in the estimation of variables directed related to precipitation, the combined technique also provides

estimates of the cloud water content, through variable x_c. The error histogram of the estimated relative to the actual x_c, i.e. the first component in an EOF representation of the cloud water content profile, is also presented in Fig. 1. For the sake of comparison, we assume that in the absence of radiometer observations the best estimate of x_c is its mean over the whole cloud model database. It may be noted in Fig.1 that the combined technique significantly improves the estimation of x_c (the relative root mean square error decreases from 100%, i.e. no skill relative to "climatological" estimates, to about 50%). It should be mentioned that retrievals with larger number of variables, i.e. more than two, to describe the cloud water content profiles have been attempted. They have not yielded better results, which suggests that there is not enough information in the radiometer observations to refine the estimation of cloud profiles through the consideration of additional orthogonal functions.

In Fig.2, a qualitative representation of the retrieved surface rainfall and mean cloud water is shown. The surface rainfall error and the actual cloud water are shown as well. The largest errors in surface rainfall occur at the boundaries of the retrieval domain, which is expected since the areas close to boundaries are poorest in radiometric information. That is, the brightness temperatures in those areas depend on profiles not in the retrieval domain and are, consequently, not considered in the retrievals, while the brightness temperatures that are considered in the retrieval only weakly depend on the profiles close to boundaries. This indeterminacy problem does not occur in situations when the whole precipitation domain is included in the retrieval domain. In general, the rain errors appear to be less than 20%, which indicates a good performance of the retrieval technique, given that the precipitation estimation using relationships that do not account for N_0^*'s variability could lead to errors as large as 100% (Testud et al. 2000).

The agreement between the retrieved and actual cloud water fields is also fairly good. The retrieved field appears to be smoother and spatially less variable, which is a consequence of the

resolution of the instrument. That is, the lower-resolution, radiometric observations provide most of the information in the combined retrieval of cloud water structures.

As mentioned above, other error structures in SRT PIA estimates are considered as well. It appears that the difference between combined and radar-only retrievals is negligible from the precipitation point of view when the decorrelation distance of the SRT PIA errors decreases below 15 km. This suggests that the radiometer information is insufficient in such cases, given the low resolution of the radiometer observations most related to PIA, to augment the information provided by the surface return technique. However, the estimates of the cloud water content are still significantly better than climatological estimates (50%-60% errors). Based on this, it may be stated that combined retrievals are noticeably superior from the precipitation point of view to radar-only retrievals when the errors of PIA estimates exhibit correlation distances similar to the radiometer's low-frequency channel resolution. Also, the combined retrievals are always more complete and consistent with all observations. The next section is devoted to the application of the combined technique to data originating from airborne observations.

4. Application to airborne data

In this section, airborne radar and radiometer observations are aggregated at the TRMM sensors' resolutions, the retrieval technique is applied to the synthesized data and the retrievals are analyzed. Airborne data present the advantage that, while being real and providing opportunities for more conclusive tests, they are free of some of the complications caused by different resolutions and sampling strategies specific to real satellite observations. Combined retrievals from active and passive airborne observations were investigated in various studies in the past. However, their conclusions may not be directly extrapolated to satellite data because the resolution of observations at frequencies where

absorption dominates is low and this may potentially affect the quality of information. This justifies investigations such as the one in this section.

The data originate from the Fourth Convection and Moisture Experiment (CAMEX-4) which took place in Florida in August - September 2001. In particular, data collected by the ER-2 Doppler Radar (EDOP) and the Advanced Multichannel Microwave Precipitation Radiometer (AMPR) are used. Details on these instruments may be found in Heymsfield et al. (1996) and Spencer et al. (1994). Observations from the Airborne Rain Mapping Radar (ARMAR) coincident with AMPR observations would probably have been more suitable for investigation of the combined technique, given ARMAR's similarity to the TRMM PR (Durden et al. 1994). However, no flight legs containing ARMAR and AMPR coincident data that are long enough to provide sufficient observations for a meaningful analysis at the TRMM resolution have been found. Consequently, we resort to EDOP and AMPR coincident data.

Fig. 3 shows a representation of the data collected by EDOP and AMPR during a flight leg on September 18, 2001 (Hurricane Erin). Superimposed on the original AMPR observations are the TRMM like synthesized observations. It may be noted in Fig. 3 that the information provided by the 10 and 19 GHz channels is significantly degraded at TRMM resolution. The high frequency channels (37 and 85 GHz) provide high-resolution observations, but the relationships between these observations and precipitation are weaker than those at lower frequencies. The EDOP observations are re-sampled at PR resolution and used in the retrievals along with the TRMM-like passive observations synthesized from the AMPR data. The SRT PIAs are not considered as information in the retrievals for two reasons. First, the PIA at EDOP's frequency (9.6 GHz) is significantly lower than that at 13.8 GHz, which is the frequency considered in the previous section and also the TRMM PR's frequency. This makes the EDOP's SRT based estimates of PIA less reliable than TRMM PR's and their value of

limited utility for low intensity rainfall. Second, the SRT PIA estimates may be used independently (at least for large attenuation profiles) for evaluation of the combined retrievals. Consequently, we choose to use the SRT PIAs to interpret the realism of the combined retrievals.

Fig. 4 contains a representation of the retrieved brightness temperatures at the initial AMPR resolution. Results show that the combined formulation allows for the retrieval of brightness temperatures at resolutions higher than that of the observations. This is because the high-resolution radar observations are available. The agreement between the observed brightness temperatures and the ones retrieved through the combined technique demonstrates the consistency of radar and radiometer observations as well as that of the models used in the retrieval. Some oscillations, which are most likely the effect of ill conditioning (more independent unknowns than independent observations), are apparent, especially in areas with low intensity rainfall. When the cloud water content is specified as a variable for each profile considered in the retrieval, some unrealistic estimates of this variable are obtained. That is, higher cloud water contents than those expected are retrieved in some low intensity rain areas, while in other high intensity rainfall areas zero cloud water content is retrieved. This suggests that the variability in the surface wind speed and the uncertainties in radiative transfer modeling might have a larger effect on retrievals than expected based on the synthetic retrieval experiment. Consequently, a single cloud variable for all profiles is considered in the retrieval.

Presented in Fig. 5 are various retrieved variables as a function of time. These include the PIA, the ratio of retrieved N_0^* to a reference value, namely N_0^* =0.08 cm^{-4}, and the vertically integrated liquid (VIL) content. PIA estimates from the SRT are also presented in the figure. It may be noted that the retrieved PIAs are in fairly good agreement with the SRT estimates, especially in the areas characterized by large attenuation. The SRT estimates are determined by considering a single value (constant for the whole leg) of the surface return in rain free areas. A more flexible and adaptive SRT

estimation such as that employed in TRMM PR algorithm (Meneghini et al. 2000) is not considered for EDOP data, given the absence of off-nadir information. The surface return varies significantly as a function of the surface wind speed, which makes the PIA estimation subject to errors in cases with strong variations in surface wind speed. For the investigated case, we set the rain free surface return based on the observations before the 15:55 and after18:26 which correspond to rain free areas. This leads to an overestimation of SRT PIA near the eye due to increased surface wind speed that causes a reduction in the surface return. Alternatively, we could set the rain free surface return based on the EDOP observations in the eye, but this would not lead to overall more accurate SRT estimates. This dilemma concerning the optimal strategy of determining the rain free surface return illustrates the need for additional information such as the radiometric observations. Also, the SRT PIA estimates in Fig.5 suggest that there is a spatial correlation in SRT PIA errors (they may be consistently positive or negative as a function of surface wind speed, which is also a variable that exhibits spatial correlation). This makes the assumptions concerning the SRT PIA errors considered in the previous section meaningful. It may be inferred from Fig. 5 that the PIA derived by the combined technique is more realistic that the SRT PIA in areas of low intensity rainfall because it does not associate large attenuation with low reflectivity profiles.

The retrieved N_0^* is characterized by large variations that are consistent, at least from the range point of view, with the results of Testud et al. (2000). It is apparent, though, that in low intensity rainfall its values tend to be unrealistically high. This tendency is probably a consequence of the fact that the algorithm attributes differences between predicted and observed brightness temperature mainly to variations in the drop size distribution and does not account for other factors such as the variability in the surface emissivity, horizontal variability of cloud water content, etc. But as already mentioned inclusion of more variables in the formulation would make the problem more ill-posed. Hopefully,

progress in the understanding and simulation of precipitation processes will allow more realistic parameterizations and more adaptive retrievals. A positive fact is that the unrealistic, large values of N_0^* in the eye do not have much impact on the overall rainfall estimation given that the reflectivity profiles corresponding to these values are characterized by very low reflectivity factors.

Presented also in Fig. 5 is the vertically integrated liquid content (VIL) as function of time. This variable appears to be strongly correlated with the PIA and the 10 GHz brightness temperature. This results from both the PIA and the 10 GHz brightness temperature being sensitive mainly to absorption (and emission given Kirkchhoff's law; Stephens 1994) by raindrops in the atmospheric column sampled by the radar or radiometer. The correlation between the PIA and the VIL suggests that errors in estimating the PIA directly translate to errors in VIL and advocates the use of radiometric information as means of reducing the uncertainty in PIA estimates and therefore in precipitation estimates.

To investigate the generality of the retrieval analysis, a second flight leg on September 23, 2001 (Hurricane Humberto) is considered. The EDOP and AMPR data (both initial and low resolution) are shown in Fig. 6. Presented in Fig. 7 are the retrieved and observed brightness temperatures at the initial AMPR resolution. The agreement between retrieved and observed values is similar to that noted in the previous case. Shown in Fig. 8 are the retrieved PIA, N_0^*, and VIL. The retrieved values indicate consistency with the conclusions derived from the analysis of the September 10 data. That is, the agreement between retrieved and SRT PIAs is good, especially for large values, N_0^* exhibits a range and variation similar to those noted before, and the VIL is strongly correlated with the PIA and the 10 GHz brightness temperature. Also, the lower-valued SRT PIA estimates seem to be affected by variations in the surface wind speed. Unlike the previous analysis, a quite systematic trend is apparent in N_0^* values. The N_0^* values tend to decrease with the range from the eye wall, although

the fluctuations are still large. This trend may be the consequence of increasing predominance of stratiform processes conducive to larger drops away from the eye wall.

The analysis of the airborne observations suggests the feasibility of the retrieval technique's application to real data. Although some artifacts are apparent, such as unrealistic N_0^* estimates in very low intensity precipitation areas, the technique provides framework for introducing additional information to mitigate uncertainties in PIA estimates. In the next chapter, an illustration of the technique's applicability to TRMM data is provided.

5. Application to TRMM data

The potential of the retrieval technique in satellite rain estimation is illustrated by its application to TRMM data. Several cases were considered, but results from only one case are presented here, given that no notable differences from case to case were observed. Nevertheless, a considerably larger number of cases must be analyzed for a comprehensive assessment of the technique's performance in satellite applications. Such an analysis is in progress, and the results will be reported separately. In this section only the technique's feasibility and the consistency of its behavior relative to the results of previous sections are investigated.

The radar algorithm used in the retrieval is fully consistent with the TRMM PR algorithm. It uses the same vertical structure characterized by five nodes that describe the hydrometeor phase and the vertical variability in reflectivity vs. attenuation and reflectivity vs. precipitation relationships (Iguchi et al. 2000). The rain type classification is also the same used by TRMM PR algorithm. The TRMM PR algorithm updates the reflectivity-precipitation relationships as a function of a parameter ε defined as (Iguchi et al. 2000)

$$\varepsilon = \frac{1 - 10^{\beta PIA_e/10}}{0.2\ln(10)\beta \int_0^{r_s} \alpha(s) Z_m^{\beta}(s) ds} \qquad (2)$$

where PIA_e is the imposed ("final value") value of PIA, $\alpha(s)$ and β are the multiplicative coefficient and the exponent in range-dependent attenuation-reflectivity relationships, s is the range, r_s is the range corresponding to the surface and $Z_m(s)$ is the attenuated reflectivity at range s. PIA_e is determined based on a bayesian formulation from the Hitschfeld - Bordan PIA, corresponding to an analytical solution of the radar equation, and the SRT PIA (Iguchi et al. 2000).

In our approach, ε is determined iteratively from radiometer observations. Specifically, $\varepsilon = \delta N_0^{*(1-\beta)}$, where δN_0^* is the ratio of the actual N_0^* to the reference N_0^* used to derive the attenuation-reflectivity relationships. The values of ε and, consequently, the simulated TMI brightness temperatures are iteratively adjusted until a minimum of the functional in (1) is attained. Our estimates differ from the TRMM PR official estimates only in the way ε is specified, which facilitates an objective analysis of the impact of using radiometric information in the TRMM PR algorithm. The consistency of TRMM PR parameterizations with those derived to predict absorption, emission and scattering properties at TRMM TMI's frequencies as a function of hydrometeor contents is achieved through the use of equivalent normalized gamma DSDs (Ferreira et al. 2001). That is, the normalized gamma DSDs that would yield the same relationships as those used by the TRMM PR algorithm are determined and used further to express the scattering property variables as functions of hydrometeor contents.

The application presented in this section is based on data from a TRMM overpass of Hurricane Bonnie on 22 August 1998. From TMI, only the 10 GHz brightness temperatures are used in the retrieval. Although strongly correlated with the actual observations, the 19 to 37 GHz simulated

brightness temperatures appear to be slightly biased. Because the formulation in (1) applies only to models that do not exhibit systematic errors, we decided to not include the 19 to 37 GHz information in the retrieval. The nature of the observed bias is under investigation. Also the 10 GHz and 85 GHz pieces of information are almost complementary, inasmuch as "pure" emission is observed at 10GHz and "pure" scattering is observed at 85GHz. This makes the formulation separable when the 19 to 37 GHz information is not used. That is, a retrieval of N_0^* (or ε) can be performed based on 10 GHz observations, followed by a retrieval of x_s based on 85GHz observations. Here, the retrieval based only on 10 GHz is presented, given that N_0^* is the variable that strongly influences the precipitation estimates below the melting layer.

Selected retrieved parameters are presented in Fig. 9. The top left panel of this figure is a contour plot of the PIA estimated using the TRMM PR algorithm (one of the TRMM 2A25 products). Shown in the top right panel are the differences between the combined technique PIA and the 2A25 PIA. As described above, the differences result from different ε estimates from the present technique based on radiometric observations. As seen in the panel, the PIA differences between the two retrievals are not large. They are within the limits of SRT PIAs uncertainties, but nevertheless they impact the values of the retrieved hydrometeor contents. Frequency plots of the 2A25 ε and the combined retrieval ε are shown in the bottom left panel of Fig. 1. It may be noted that the ε values from the combined technique exhibit larger deviations from 1.00 than the 2A25 values. The 2A25 values seem to be more conservative, i.e. closer to 1.00. This may be an indication of less information incorporated by the TRMM PR algorithm, given that this algorithm weighs the SRT PIA estimates as a function of their reliability, and when the reliability is small the nominal values are highly weighted. A representation of retrieved VILs vs. 2A25 VILs is given in the bottom right panel of Fig.9. A strong correlation between the two types of estimates is noted; however, the combined retrieval VILs are

systematically larger, especially for low values below (5 kg/m^2). Overall, the combined retrieval estimates are about 16% larger than the 2A25 estimates. It should be mentioned that the root mean squared difference (RMSD) between 2A25 PIAs and the SRT PIAs (determined also by the TRMM PR algorithm) is the same as the RMSD between the combined retrieval PIAs and SRT PIAs. Therefore, although the combined method is as consistent with the SRT PIA estimates as the TRMM PR algorithm, it produces results that are systematically different from those of 2A25 algorithm. This is a consequence of the highly nonlinear relationships among the variables involved in the algorithm, and suggests that apparently similar retrievals may lead eventually to systematically different results. Further, it is possible that some of the differences between the official TMI and PR algorithm estimates may originate in the lack of reliable PIA estimates for low intensity rainfall which may lead to conservative PR estimates (ε=1) that are not necessarily always in agreement with the actual DSDs.

Displayed in Fig. 10 are scatter plots of observed brightness temperatures (10 and 19 GHz) vs. brightness temperatures simulated based on the two types of hydrometeor content estimates, namely, the combined retrieval and the 2A25 estimates. The differences between the simulated temperatures and observations are reduced in the combined retrieval case, especially at the 10 GHz (about 20% reduction in RMSD). The 19 GHz combined estimates also show smaller deviations (about 9% RMSD), although the 19 GHz information is not used in the retrieval. This suggests that the improvement in the 10 GHz temperature retrieval is not just a consequence of the minimization associated with the technique but encompasses an improvement at the level of retrieved hydrometeor contents.

Other cases we investigated gave similar results. That is, the combined precipitation estimates are higher than the 2A25 estimates by about 10% to 15% and the agreement between the retrieved PIAs and SRT PIAs is similar to that between the 2A25 PIAs and SRT PIAs. Also, the improvement

in the 10 GHz temperature prediction translates to a somewhat smaller improvement in the 19 GHz temperature prediction. However, it is premature to state whether the application of the combined technique to TRMM data will consistently yield larger precipitation estimates. Considerably larger data sets are needed to address this issue. Moreover, the consistency of radiative transfer calculations with real observations should be more comprehensively investigated, and the retrieved variables must be evaluated with respect to independent observations, e.g. ground radar observations, disdrometer data, etc..

6. Conclusions

A method for estimating precipitation profiles from multifrequency, multiresolution, active and passive microwave observations is formulated and investigated in this paper. The method is based on physical models that simulate, starting from active observations and a set of free parameters, the passive observations. The free parameters are determined such that an agreement between simulated and observed variables as well as agreement between retrieved and expected properties is achieved. The method is tested using synthetic and airborne data and an illustration regarding its possible application to satellite data is provided.

The synthetic retrieval experiment uses cloud resolving model data to generate passive and active observations characterized by TRMM instruments' resolutions and frequencies. Retrievals are performed and analyzed. Results show that the inclusion of passive information in retrievals may reduce the uncertainties in PIA estimates. Improvements in PIA estimates translate to improvements in precipitation estimates. That is because the PIA estimates strongly influence the precipitation retrieval not only through attenuation-corrected profiles of reflectivity but also through the relationships used to relate the corrected profiles to precipitation. Even though the microwave sensor

passive information is characterized by low resolution, it is nonetheless effective in mitigating errors in SRT PIA estimates in some situations. When SRT PIA estimates are affected by purely random errors, the passive information has little impact on precipitation retrievals. When these SRT PIA errors are correlated on distances on the order of magnitude of the low-frequency channels' resolutions, the benefit of passive observations is evident.

The analysis of airborne data suggests that SRT PIA errors are not purely random but exhibit some spatial correlation. To make the analysis consistent with the synthetic retrieval experiment and relevant for satellite applications the airborne data are aggregated at the TRMM instruments' resolutions. Retrievals show the technique's ability to restore the radiometric information at the initial (airborne instrument's) resolution. The SRT information is not included in the retrieval (given its information poor content at the EDOP's frequency and the need for validation of retrieved variables) but is used to evaluate the combined retrieval PIA. Results indicate a good agreement of retrieved PIAs with SRT PIAs. Although some artifacts in estimated parameters are apparent, refined and additional parameterizations and additional constraints should help to eliminate these.

The technique's application to TRMM data shows its feasibility when dealing with real satellite observations. Although more detailed investigations are to be performed to reach definite conclusions, the results are encouraging. Values of retrieved parameters are similar to those derived from the TRMM PR algorithm in terms of some variables, while others are different. These differences may be systematic and caused exclusively by the different information content used by the two algorithms and the nonlinear relationships among the variables involved in retrievals. That is, the SRT PIA seem to have a weaker influence on retrieved parameters in the TRMM PR algorithm than radiometric information has in the combined technique. As a result, in this study the precipitation estimates from

the combined retrieval are larger than those from the TRMM PR. Whether the combined retrievals lead in general to larger estimates than the PR-only estimates remains to be investigated.

Future work must be done to analyze the technique's utility and performance in satellite applications. As already stated this implies applications to a large set of real TRMM observations and comparison of the results with 2A25 products. Also data from field experiments should be included in the analysis. These data are particularly useful because they may provide additional insights related to the validity of different estimates such as the DSD intercept, the cloud water content, and the mixed hydrometeor properties. For example, disdrometer data may characterize the range of expected DSD parameters for given meteorological contexts. Ground radar data and kinematic retrievals could be used to estimate the cloud water fields, while multiple frequency radar observations of mixed-phase hydrometeors may better depict their structure. All these elements considered together may provide a comprehensive analysis of the technique formulated and preliminarily investigated in this study for the purpose of microwave rain estimation applications.

Acknowledgments: The authors acknowledge and appreciate useful discussions with Drs. Robert Meneghini and Lin Tian of NASA/GSFC. The cloud model data were provided by Dr. Scott Braun of NASA/GSFC. The study was supported by the NASA TRMM Project.

References

Bauer, P., L. Schanz, L. Roberti, 1998: Correction of Three-Dimensional Effects for Passive Microwave Remote Sensing of Convective Clouds. *J. Appl. Meteorol.*, **37**, 1619-1643.

Durden, S. L., E. Im, F. K. Li, W. Ricketts, A. Tanner, and W. Wilson, 1994: ARMAR - an airborne rain-mapping radar. Journal of Atmospheric and Oceanic Technology, **11**, 727-737.

Ferreira, F., P. Amayenc, S. Oury, and J. Testud, 2001: Study and Tests of Improved Rain Estimates from the TRMM Precipitation Radar. *Journal of Applied Meteorology*, **40**, 1878–1899.

Grecu, M., and E. N. Anagnostou, 2002: Use of Passive Microwave Observations in a Radar Rainfall-Profiling Algorithm. *Journal of Applied Meteorology*, **41**, 702–715.

Haddad, Z. S., E. A. Smith, C. Kummerow, T. Iguchi, M. R. Farrar, S. L. Durden, M. Alves, and W. S. Olson, 1997: The TRMM 'day-1' radar/radiometer combined rain-profiling algorithm. *J. Meteorol. Soc. Japan*, **75**, 799-808.

Harris D, and Foufoula-Georgiou, 2001: Subgrid variability and stochastic downscaling of modeled clouds: Effects on radiative transfer computations for rainfall retrieval. *J Geophys Res-Atmos*, **106**, 10349-10362.

Heymsfield G. M., S. Bidwell, I. J. Caylor, S. Ameen, S. Nicholson, W. Boncyk, L. Miller, D. Vandermark, P. E. Racette, and L. R. Dod, 1996: The EDOP radar system on the high-altitude NASA ER-2 aircraft. J. Atmos. Oceanic. Tech., 13, 795-809.

Iguchi, T., T. Kozu, R. Meneghini, J. Awaka, and K. Okamoto, 2000: Rain-profiling algorithm for the TRMM precipitation radar. *J. Appl. Meteorol.*, **39**, 2038-2052.

Kummerow, C., W. Barnes, T. Kozu, J. Shiue, and J. Simpson, 1998: The tropical rainfall measuring mission (TRMM) sensor package. *J. Atmos. and Ocean Tech.*, **15**, 808-816.

Marzano, F. S., A. Mugnai, G. Panegrossi, N. Pierdicca, E. A. Smith, and J. Turk, 1999, Bayesian estimation of precipitating cloud parameters from combined measurements of spaceborne microwave radiometer and radar. *IEEE Transactions on Geoscience And Remote Sensing*, **37**, 596-613.

Meneghini, R., H. Kumagai, J. R., T. Iguchi, and T. Kozu, 1997: Microphysical retrievals over stratiform rain using measurements from an airborne dual-wavelength radar-radiometer. *IEEE Transactions on Geoscience and Remote Sensing*, **35**, 487-506.

Meneghini, R., T. Iguchi T., T. Kozu, L. Liao L., K. Okamoto, J. A. Jones, and J. Kwiatkowski, 2000: Use of the surface reference technique for path attenuation estimates from the TRMM radar. *Journal of Applied Meteorology*, **39**, 2053-2070.

Olson, W. S., C. Kummerow, G. M. Heymsfield, I. J. Caylor, and L. Giglio, 1996. A method of combined passive/active microwave retrievals of cloud and precipitation profiles. *J. Appl. Meteorol.*, **35**, 1763-1789.

Olson, W. S., P. Bauer, N. F. Viltard, D. E. Johnson, W. K. Tao, R. Meneghini, L. Liao, 2001: A Melting-Layer Model for Passive/Active Microwave Remote Sensing Applications. Part I: Model formulation and comparison with observations. *J. Appl. Meteorol.*, **40**, 1145-1163.

Roberti, L. and C. Kummerow, 1999: Monte Carlo calculations of polarized microwave radiation emerging from cloud structures, *J. Geophys. Res.*, **104**, 2093-2104.

Schols, J. L., and J. A. Weinman, 1994: Retrieval of hydrometeor distributions over the ocean from airborne single-frequency radar and multi-frequency radiometric measurements. *Atmospheric Research*, **34**, 329-346.

Smith, E. A., F. J. Turk, M. R. Farrar, A. Mugnai, X. W. Xiang, 1997: Estimating 13.8-GHz path-integrated attenuation from 10.7-GHz brightness temperatures for the TRMM combined PR-TMI precipitation algorithm. *Journal of Applied Meteorology*, 36 (4): 365-388.

Spencer, R. W., R. E. Hood, F. J. LaFontaine, E. A. Smith, R. Platt, J. Galliano, V. L. Griffin, and E. Lobl, 1994: High-resolution imaging of rain systems with the advanced microwave precipitation radiometer. *Journal of Atmospheric and Oceanic Technology*, **11,** 849-857.

Weinman, J. A., R. Meneghini, and K. Nakamura, 1990: Retrieval of precipitation profiles from airborne radar and passive radiometer measurements: Comparison with dual-frequency radar measurements. *Journal of Applied Meteorology*, **29**, 981-993.

Testud, J., S. Oury, and P. Amayenc, 2000: The concept of "normalized" distribution to describe raindrop spectra: A tool for hydrometeor remote sensing. *Physics and Chemistry of the Earth. Part B-Hydrology Oceans and Atmosphere*, **25**, 897-902 .

Stephens, G. L., 1994: Remote sensing of the lower atmosphere. Oxford University Press, 523 pp.

List of Figures

Figure 10 Combined retrieval from TRMM data for August 22, 1998. Observed vs. combined algorithm and observed vs. 2A25-based brightness temperatures. Included are the 10 and 19 GHz brightness temperatures.

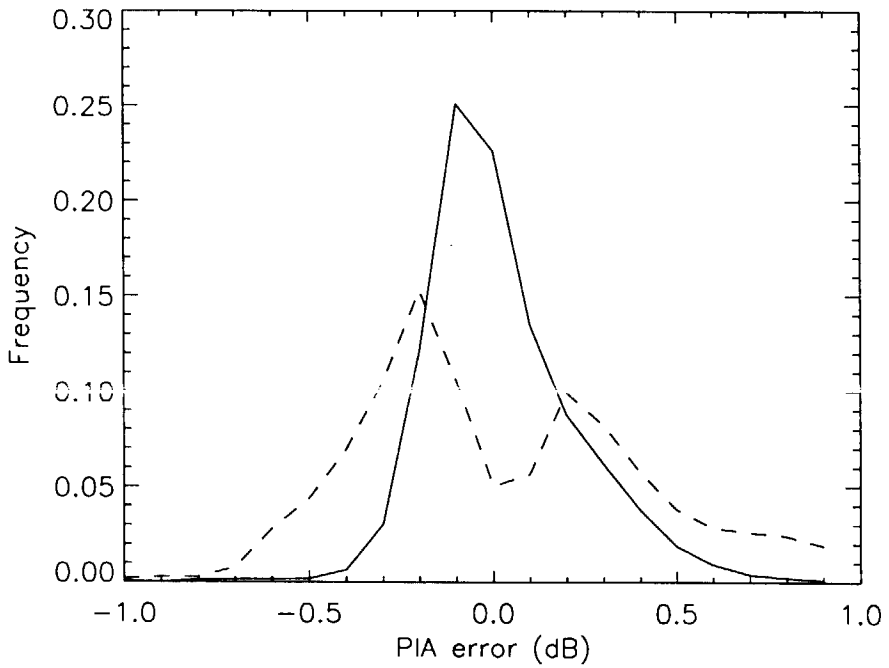
0.30
0.25
0.20
0.15
0.10
0.05
0.00
Frequency
−1.0
−0.5
0.0
0.5
1.0
PIA error (dB)

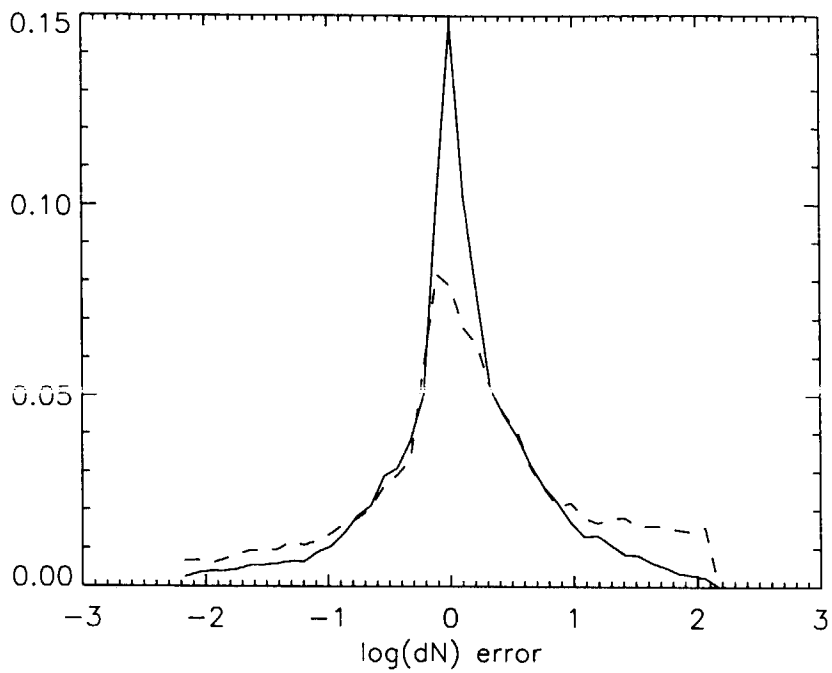
0.15
0.10
0.05
0.00
−3
−2
−1
0
1
2
3
log(dN) error

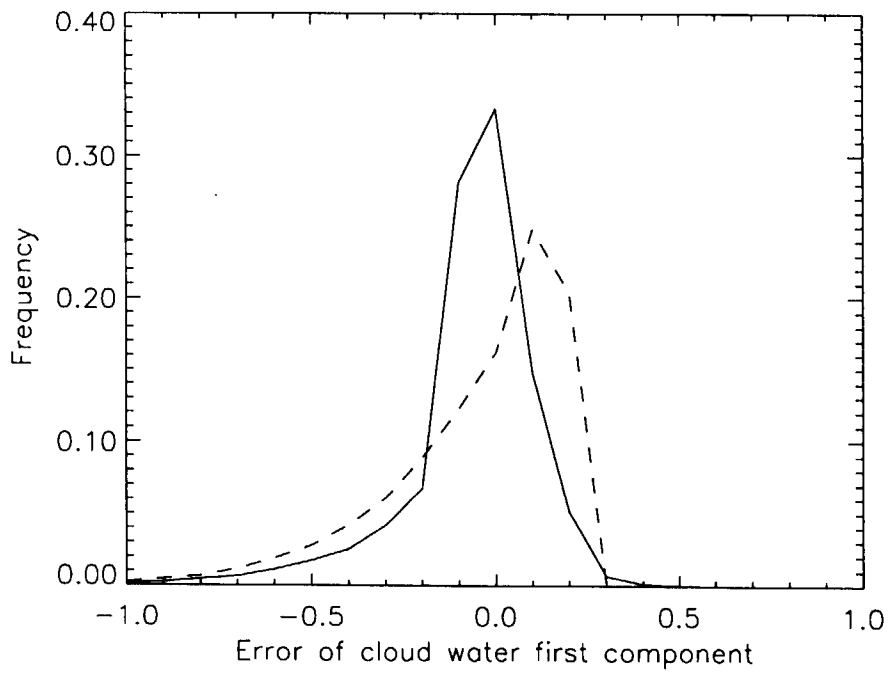
0.40
0.30
0.20
0.10
0.00
Frequency
−1.0
−0.5
0.0
0.5
1.0
Error of cloud water first component

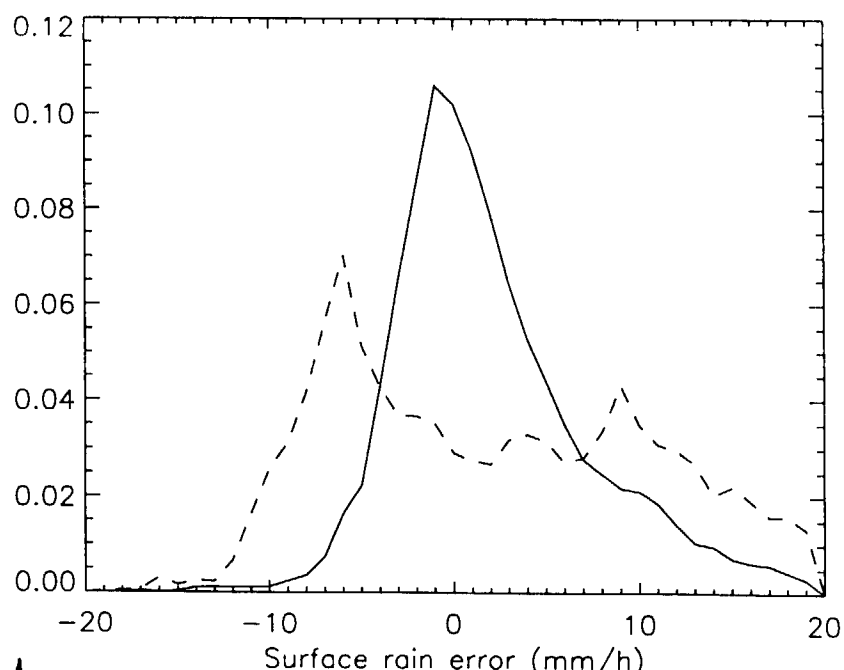
0.12
0.10
0.08
0.06
0.04
0.02
0.00
−20
−10
0
10
20
Surface rain error (mm/h)

Fig. 1

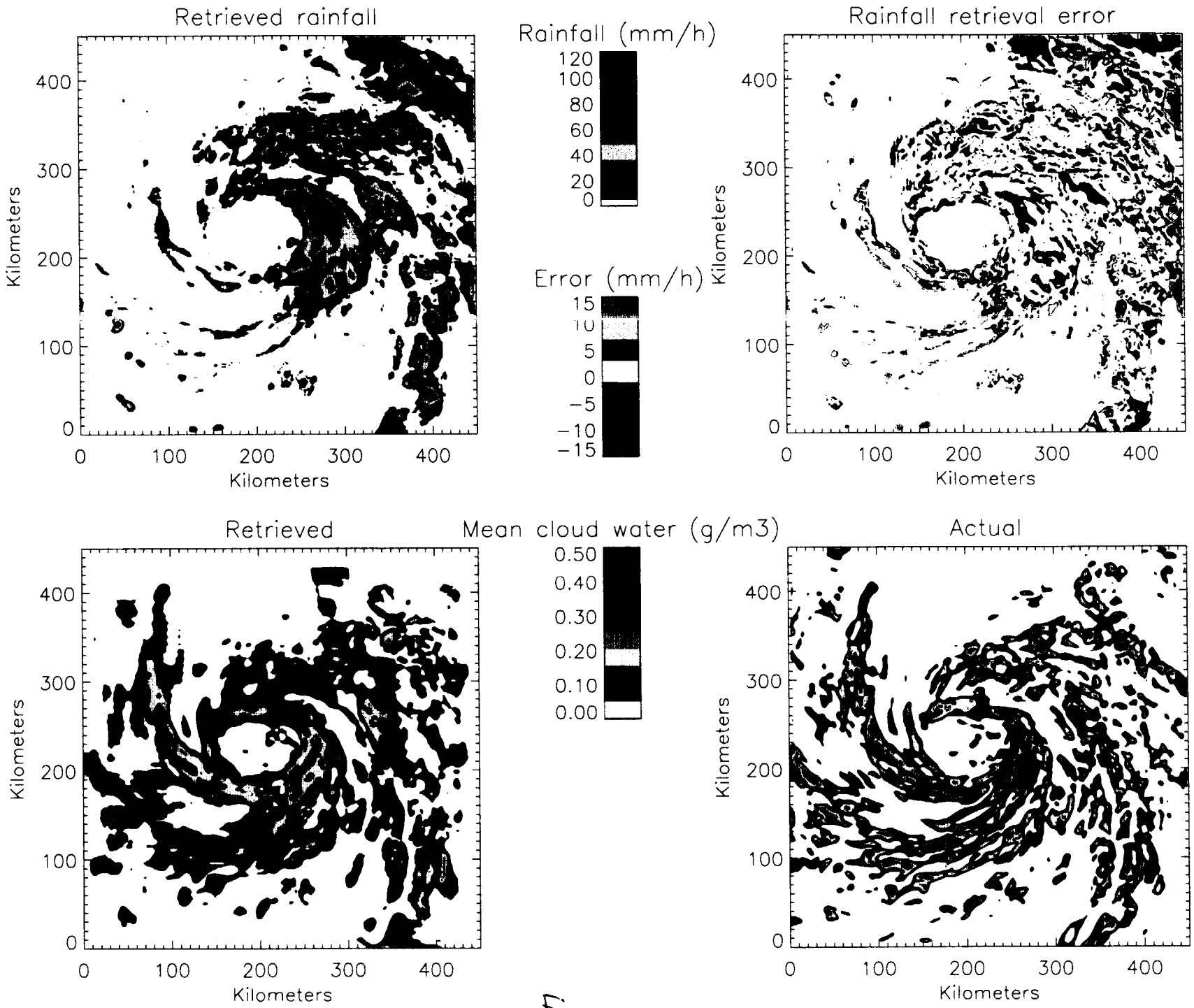
Retrieved rainfall
Rainfall (mm/h)
120
100
80
60
40
20
0
Rainfall retrieval error
Error (mm/h)
15
10
5
0
−5
−10
−15
Kilometers
0
100
200
300
400
Retrieved
Mean cloud water (g/m3)
0.50
0.40
0.30
0.20
0.10
0.00
Actual

Fig. 2

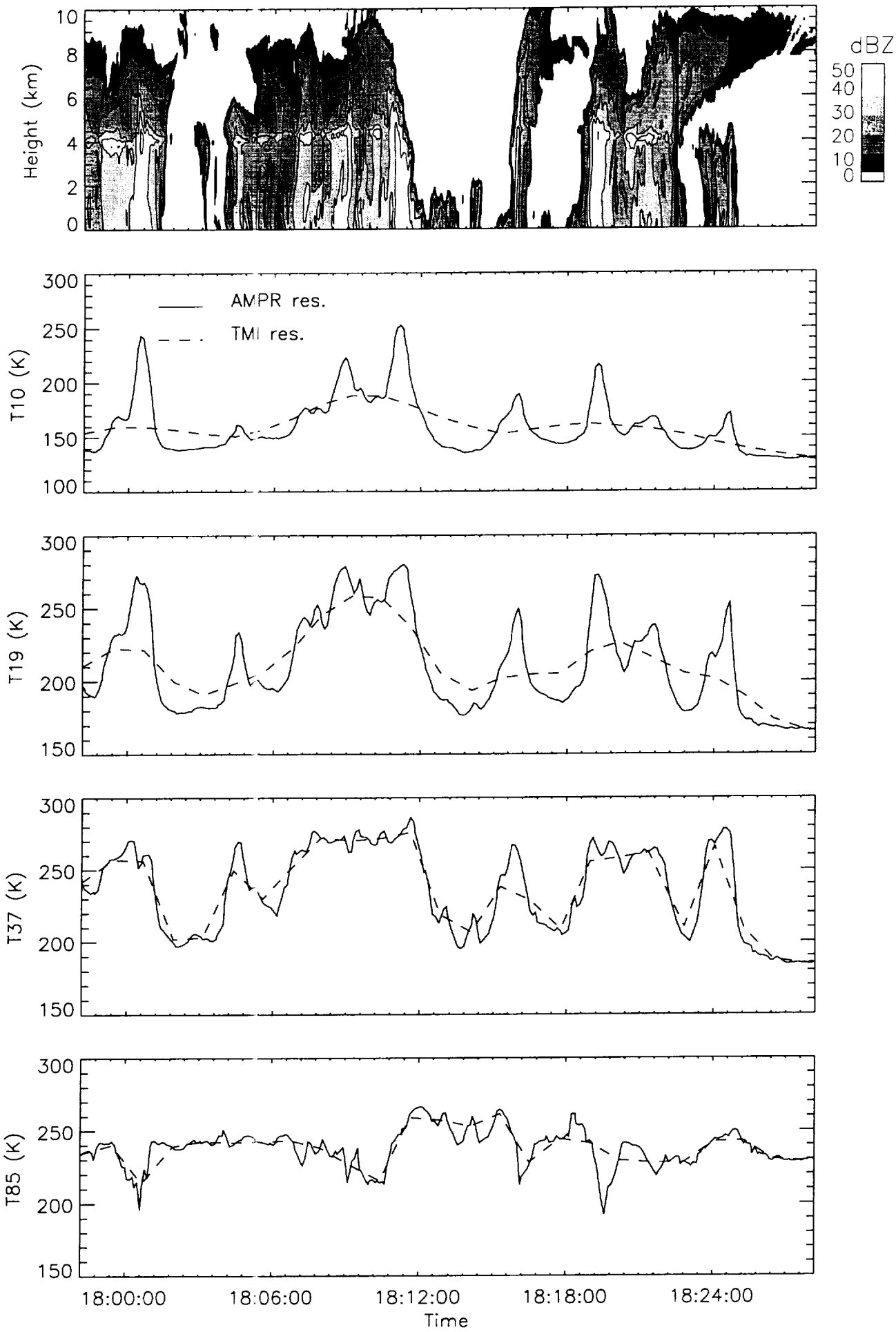
Height (km)
10
8
6
4
2
0
dBZ
50
40
30
20
10
0
AMPR res.
TMI res.
T10 (K)
300
250
200
150
100
T19 (K)
T37 (K)
T85 (K)
18:00:00
18:06:00
18:12:00
18:18:00
18:24:00
Time

Fig. 3

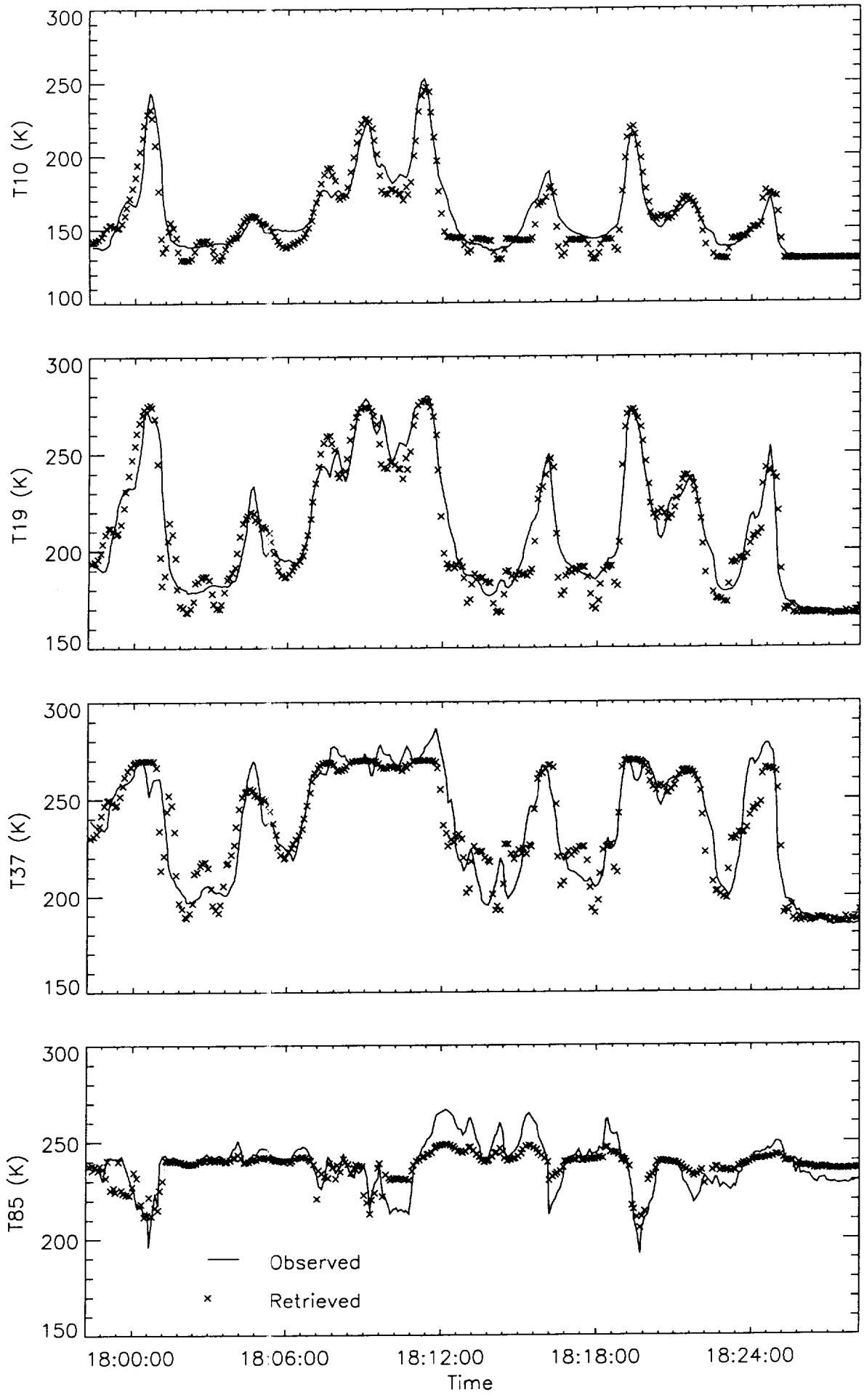
T10 (K)
T19 (K)
T37 (K)
T85 (K)
300
250
200
150
100
Observed
Retrieved
18:00:00
18:06:00
18:12:00
18:18:00
18:24:00
Time

Fig. 4

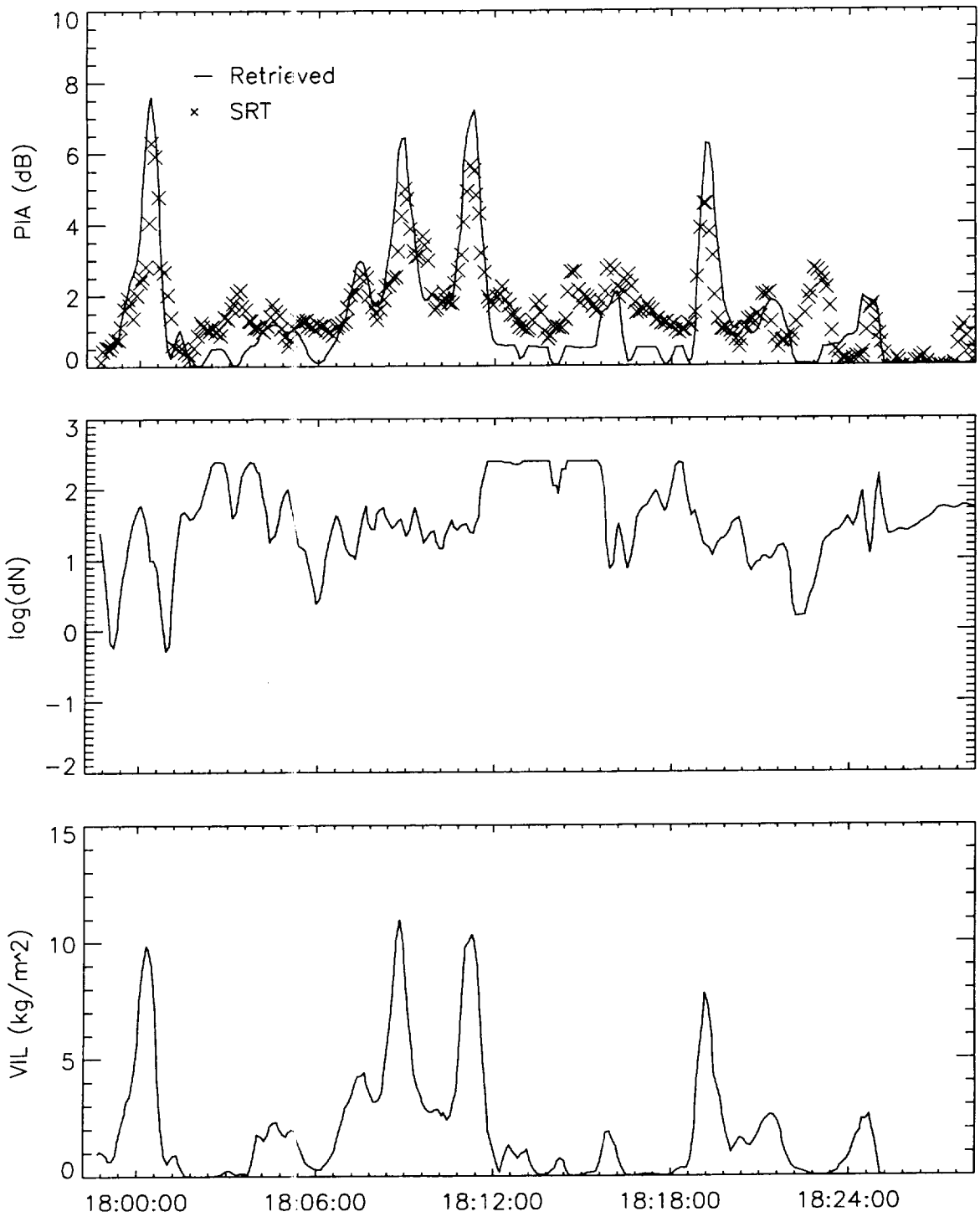
Retrieved
SRT
PIA (dB)
log(dN)
VIL (kg/m^2)
18:00:00
18:06:00
18:12:00
18:18:00
18:24:00

Fig. 5

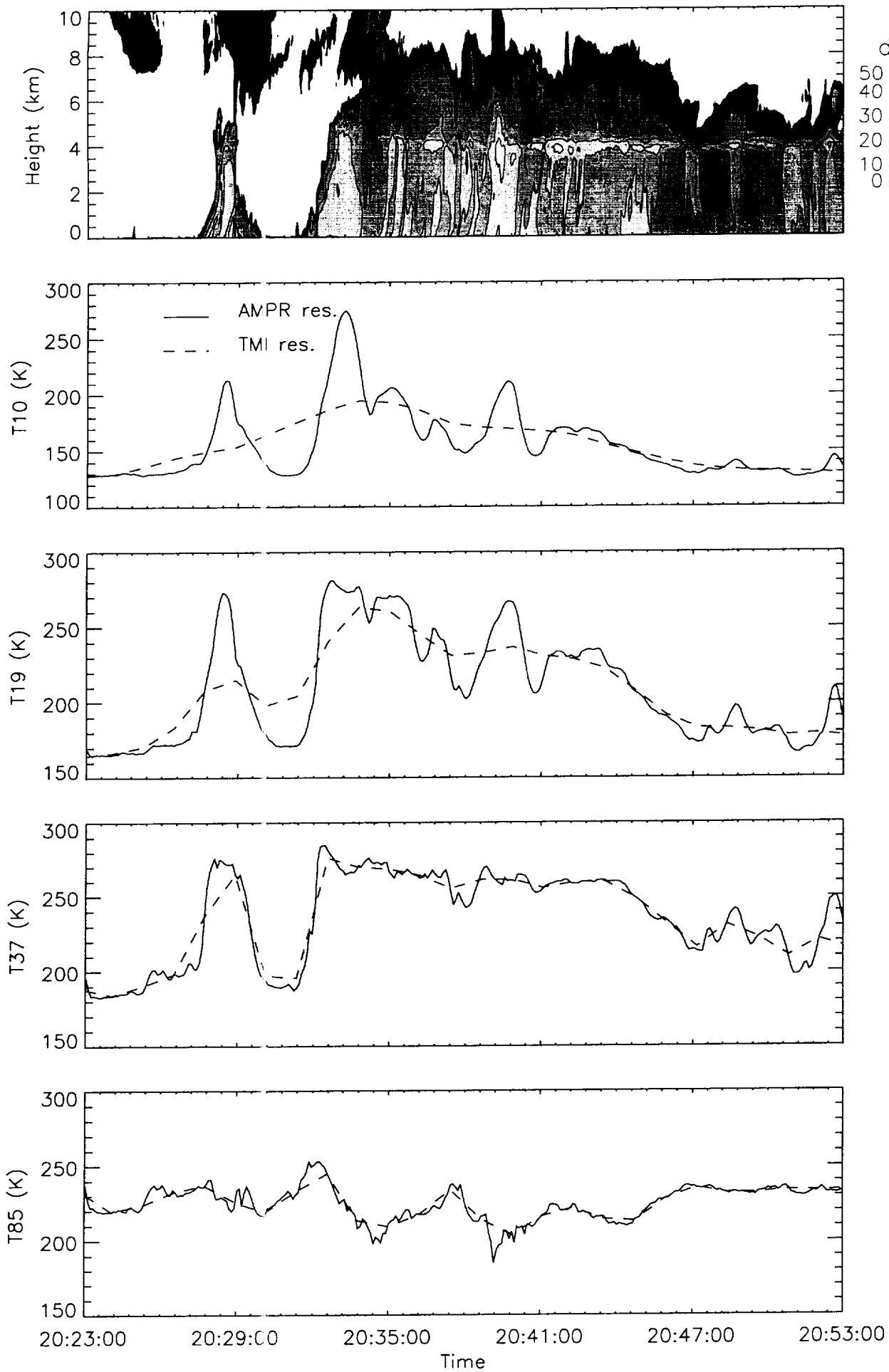
Height (km)
10
8
6
4
2
0
dBZ
50
40
30
20
10
0
AMPR res.
TMI res.
T10 (K)
300
250
200
150
100
T19 (K)
300
250
200
150
T37 (K)
300
250
200
150
T85 (K)
300
250
200
150
20:23:00
20:29:00
20:35:00
20:41:00
20:47:00
20:53:00
Time

Fig. 6

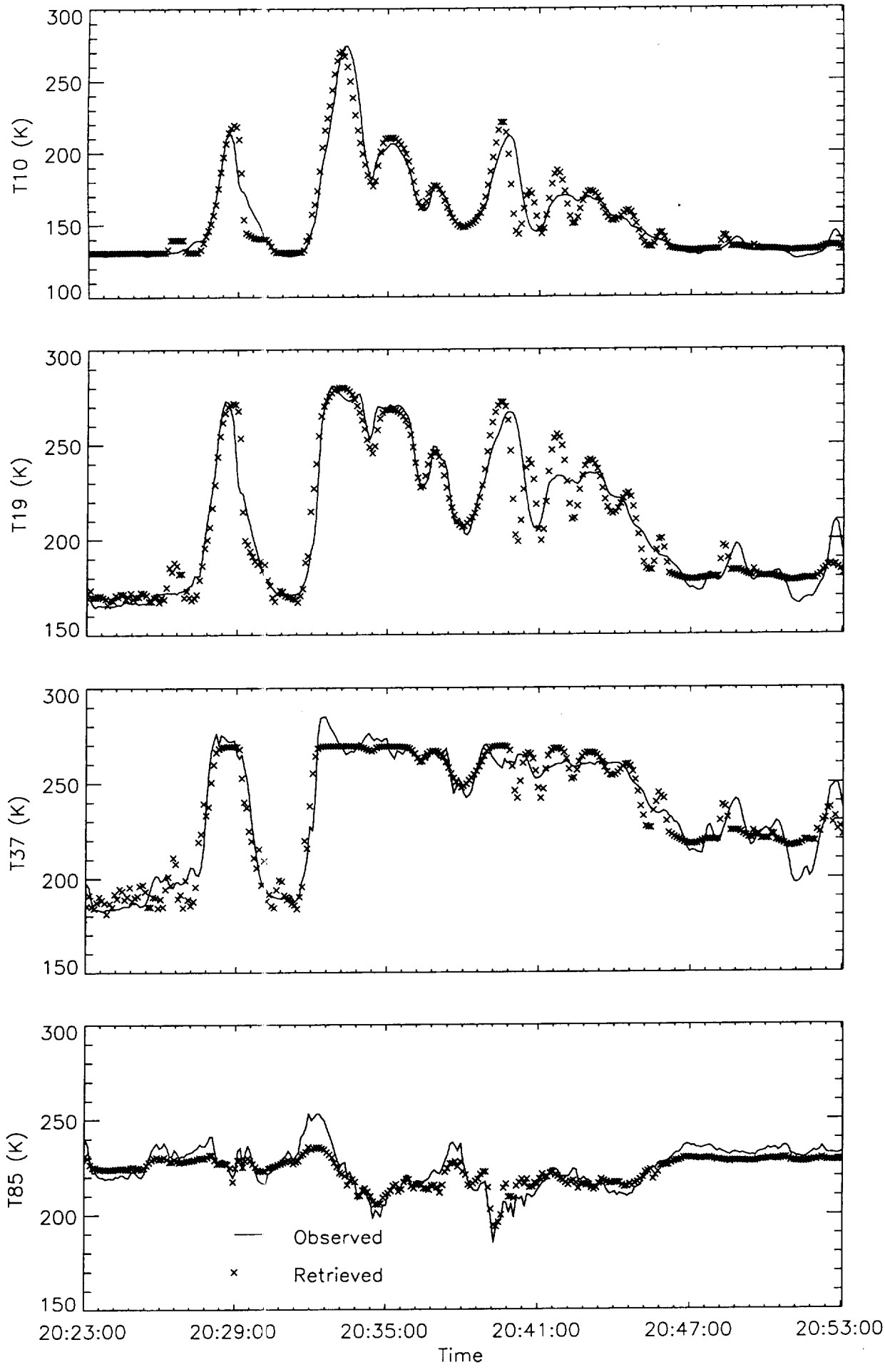
T10 (K)
T19 (K)
T37 (K)
T85 (K)
300
250
200
150
100
Observed
Retrieved
20:23:00
20:29:00
20:35:00
20:41:00
20:47:00
20:53:00
Time

Fig. 7

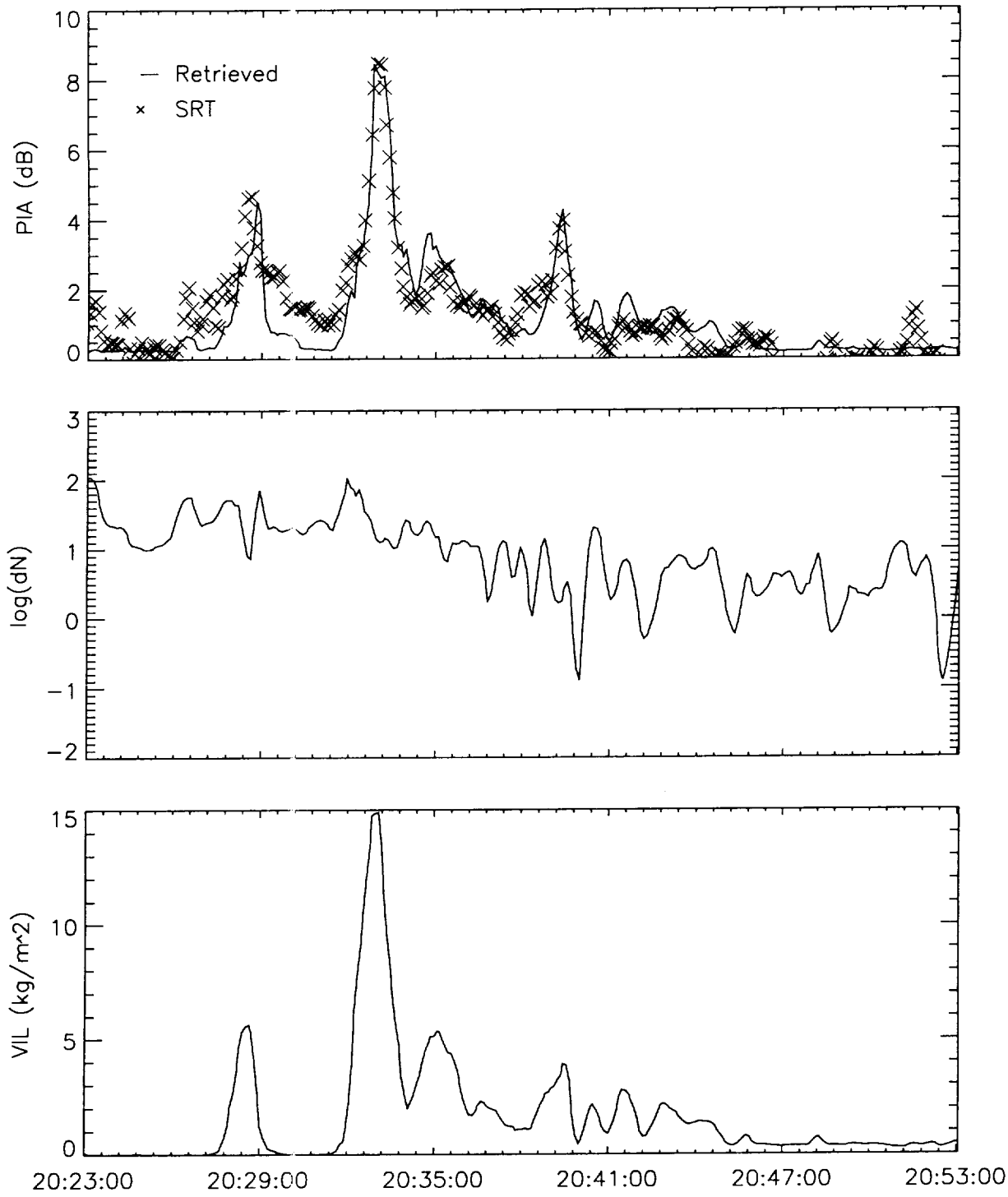
PIA (dB)
Retrieved
SRT
log(dN)
VIL (kg/m^2)
20:23:00
20:29:00
20:35:00
20:41:00
20:47:00
20:53:00

Fig. 8

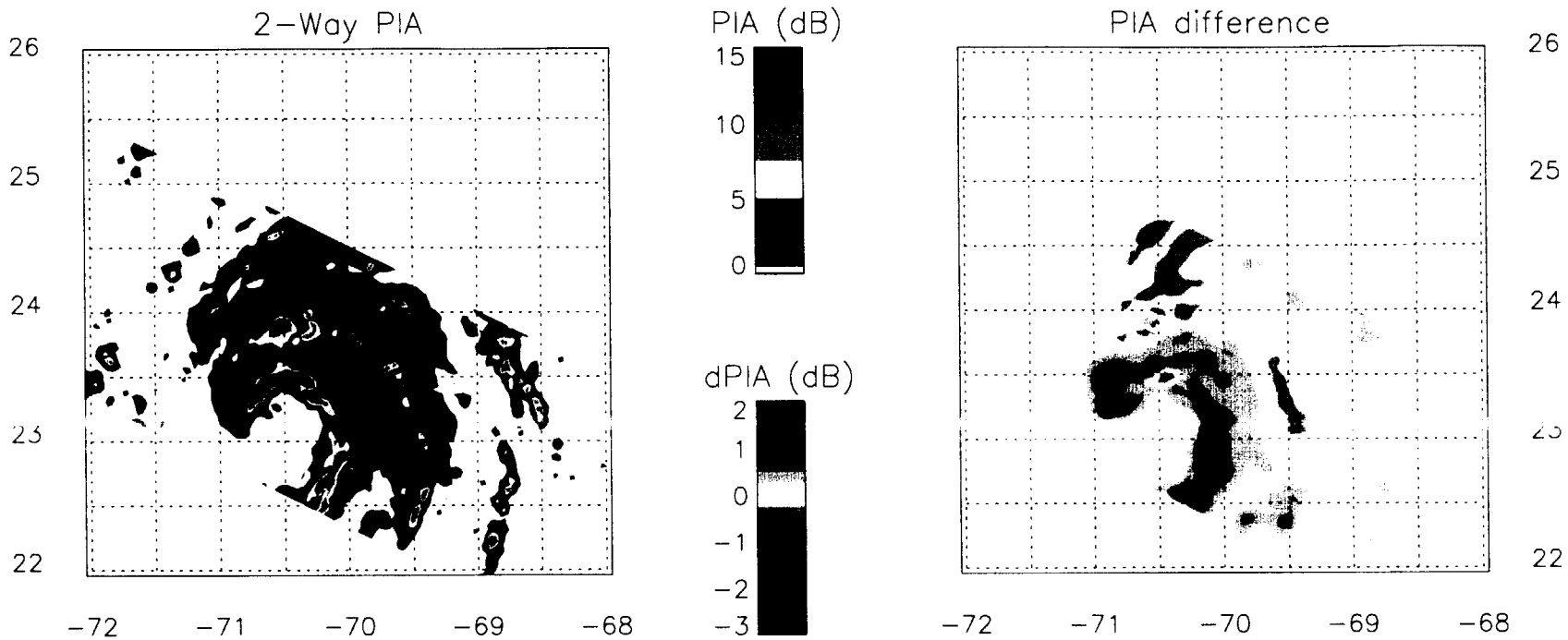
2-Way PIA
PIA (dB)
15
10
5
0
dPIA (dB)
2
1
0
-1
-2
-3
PIA difference
26
25
24
23
22
-72
-71
-70
-69
-68

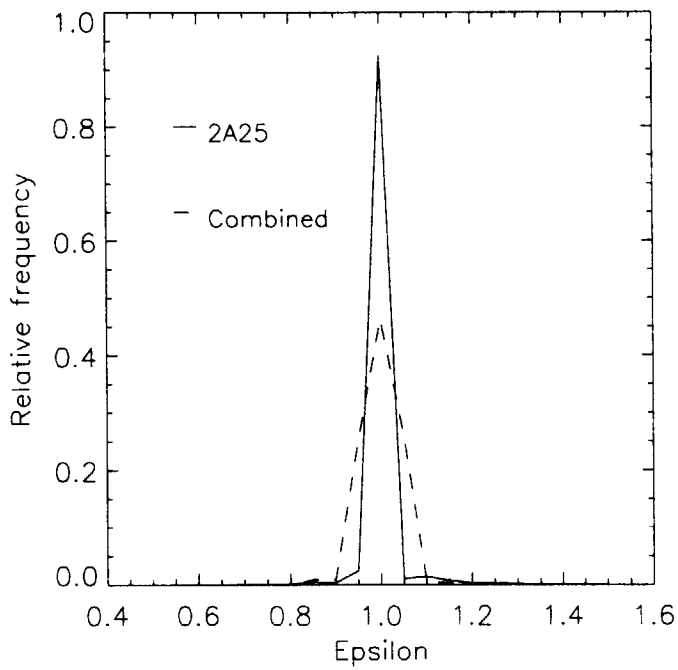
1.0
0.8
0.6
0.4
0.2
0.0
Relative frequency
2A25
Combined
0.4
0.6
0.8
1.0
1.2
1.4
1.6
Epsilon

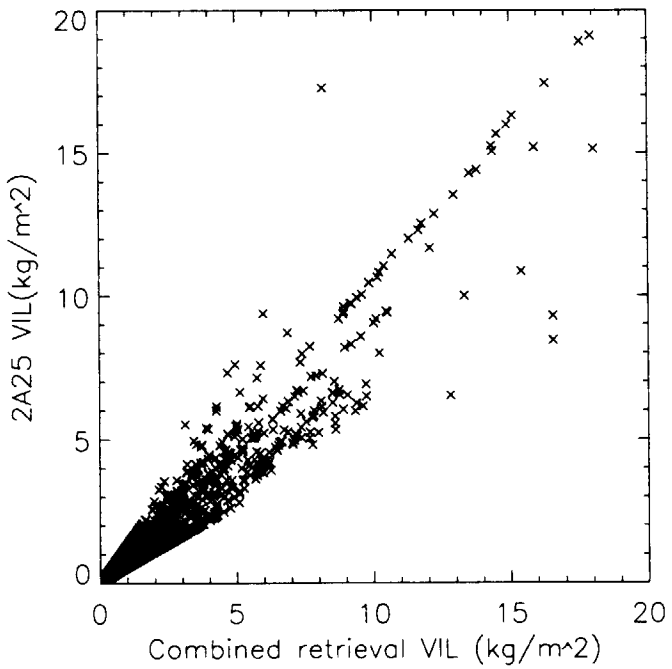
20
15
10
5
0
2A25 VIL(kg/m^2)
0
5
10
15
20
Combined retrieval VIL (kg/m^2)

Fig. 9

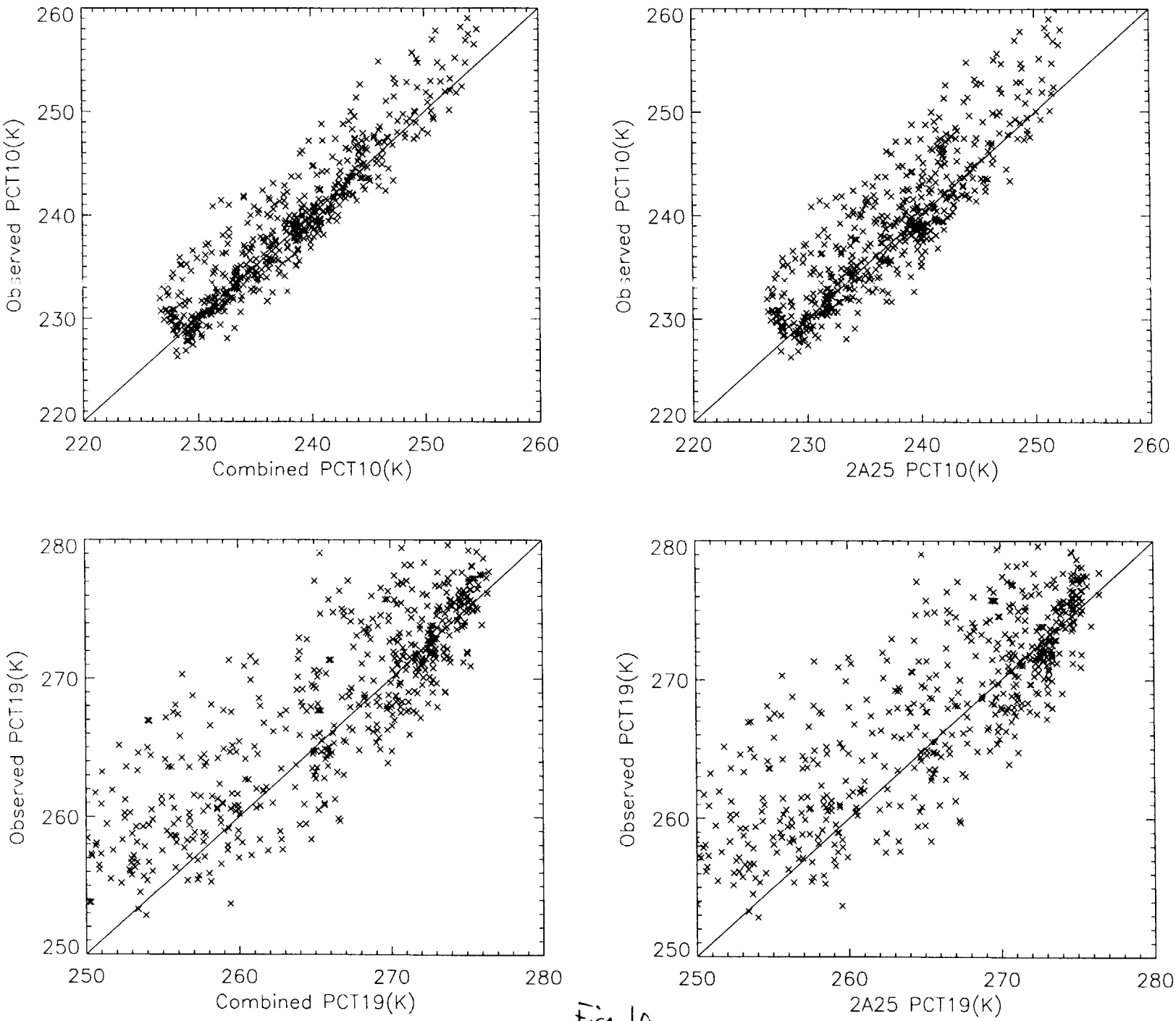
Observed PCT10(K)
Combined PCT10(K)
Observed PCT10(K)
2A25 PCT10(K)
Observed PCT19(K)
Combined PCT19(K)
Observed PCT19(K)
2A25 PCT19(K)

Fig 10

RETRIEVAL OF PRECIPITATION PROFILES FROM MULTIRESOLUTION, MULTIFREQUENCY, ACTIVE AND PASSIVE MICROWAVE OBSERVATIONS

Mircea Grecu, Emmanouil N. Anagnostou, and William S. Olson

Popular Summary

Few of the important questions regarding the understanding and prediction of earth processes can be answered without reliable estimation of global precipitation. This is why for the last five decades, since the emergence of appropriate technology, precipitation estimation at scales on the order of hundred kilometers has been a constant topic of interest for scientists and engineers. Ground instruments, given limitations in terms of area coverage, can provide only a limited portion of the big picture concerning the precipitation that we need to analyze and visualize. In these circumstances, considerable effort has been continuously devoted to the development and application of technologies that allow precipitation monitoring from space. The physics principle used to monitor the precipitation from space is simple: every object in the universe emits, absorbs and scatters radiant energy. While humans cannot visually detect the radiation emitted, absorbed, and scattered by raindrops or many other natural objects, they have devised instruments that can do that. Such instruments, called radiometers, were placed on artificial satellites to measure various portions of the energy emitted, absorbed and scattered by atmospheric particles (including raindrops) and the Earth Surface. The Tropical Rainfall Measuring Mission (TRMM) satellite is equipped with a radiometer called the TRMM Microwave Imager destined to provide observations for precipitation estimation.

The challenges in precipitation estimation from TMI observations originate from the fact that each individual observation gauges the energetic interaction of precipitation particles with radiant energy in very large atmospheric volumes. These volumes correspond to cylinders vertically extending from the earth surface to the top of the atmosphere and having the base of hundred of squared kilometers. The distribution of precipitation particles as well as their sizes vary considerably in these volumes, which makes difficult the determination of one-to-one relationships between TMI observations and the precipitation amounts. Additional information, derived from theoretical models and independent practical observations, is usually employed to develop algorithms that provide such relationships. To facilitate the development of TMI precipitation estimation algorithms, another instrument called the Precipitation Radar (PR) was devised and placed on the TRMM satellite. The PR does not rely on natural sources of energy to detect the presence of rain particle in its sampling volumes. Instead, it sends energy pulses and measures the energy returned by particles in its observation volumes. The PR sampling volumes are significantly smaller than TMI's and correspond to cylinders of 250 m height and approximately 5 km radius. Since the main back scatterers in these volumes are precipitation particles, the energy returned and measured by the PR may be used to estimate the precipitation. Given its small sampling volumes, the PR provides information considerably easier to translate to reliable precipitation estimates.

Although the PR information is usually incorporated in TMI-based precipitation estimation indirectly, through the refinement of the hypotheses and models supporting the estimation algorithm, a direct use of PR observations in TMI algorithms is possible. Or, more generally,

methodologies for precipitation estimation from PR and TMI observations may be developed. This study investigates such a methodology. The methodology is based on a procedure that adaptively changes based on TMI observations some assumptions, i.e. numerical values, in the PR estimation algorithm.

The methodology is investigated using simulated data, and airborne and TRMM observations. A numerical model able to simulate cloud and precipitation dynamics is used to generate precipitation and other fields on which the TRMM observations depend. Other models that quantitatively describe the interaction of precipitation particles with various sources of radiant energy are used to synthesize TRMM-like observations. The combined methodology is applied to the artificially generated data and the estimated precipitation fields are compared to those used in the synthesis. Results show advantages of using the combined methodology. The airborne data are provided by instruments that are similar in principle to those aboard TRMM, but different in terms of the atmospheric volumes they sample. In this sense, the airborne radiometer and precipitation radar provide significantly better resolution data. The airborne data are degraded to the satellite data resolution and the combined methodology is applied to the low-resolution data. The analysis of results indicates a good ability of the combined technique to use low-resolution information to improve the precipitation estimates from high-resolution information. The methodology's application to TRMM data reveals its feasibility in dealing with real satellite data.